Received: 3 October 2022 | Accepted: 10 October 2022

DOI: 10.1002/pamm.202200067

Growth of green wood based on a phase field model

Jan Bernd Wulf[1,*] and **Ingo Muench**[1]

[1] Institute of Structural Mechanics and Dynamics, August-Schmidt-Straße 8, D-44221 Dortmund

Tree engineering is a young discipline utilizing trees as structural elements, where the determination of limit loads in tree trunks is of great importance. Simple numerical models underestimate the load-bearing capacity of green wood in contrast to experimental bending tests. A well-known reason for this is the residual stress state of the living tree lowering compressive stress towards the trunks surface. This results in an overall stress state, which increases the load capacity, since the tensile strength of wood is commonly higher than its compressive strength. By determining the residual growth stress, a more accurate evaluation of the load-bearing capacity of a living tree is possible. The residual stress state is a non-linear and time dependent function in thickness direction of the trunk. In order to simulate growth and growth stress, a phase field model is employed.

The morphology of a tree is the result of innumerable and often temporary environmental stimuli, which also change and interact with the genetically predisposed growth tropisms. Therefore, we use image processing to capture the individual tree morphology of an existing tree, which is based within the phase field model as predefined growth direction. This is the basis for primary growth in the model. Additionally the model simulates the secondary growth, which corresponds to the thickness of the trunk. Except in tropical areas, this growth is associated with growth rings, which we assign as an attribute to the modelled material. While in the branch structure several tropisms (e.g. gravitropism) are responsible for the off-centre accumulation of woody material, in the stem region we only follow the stress-induced growth. This mechanism can respond to either the principal tensile stress or the principal compressive stress in our model, as this difference is observed in hardwoods and softwoods.

Since the wood matrix represents an anisotropic material with a distinct fiber direction, we approach it in our model by a transversely isotropic constitutive law, whose principal direction coincides with the growth direction.

1 Introduction

With regard to nature conservation and the saving of greenhouse gases, the Federal Government of Germany aims to reduce new land consumption for settlements and transport to less than 30 hectares per day by 2030 and to zero by 2050 [3]. To frame this: from 2010 to 2020, land consumption averaged about 60 hectares per day. It is therefore increasingly important to find alternative concepts for roads and buildings. One solution is to move living space to areas that do not seal the ground. In Germany there are already around fifty tree house hotels [12], where living trees are used as the main structural element for foundation. Since this becomes more and more popular a safety concept for building in living trees is overdue.

As far as centric load is concerned, the reasonable load can be well estimated. The maximum centric load capacity is high compared to the bending load capacity. In order to be able to assess the reasonable bending load well, we account for residual stresses caused by maturation of wood cells. Thibaut *et al.* [13] as well as Niklas and Spatz [9] characterize these as growth stresses acting against gravitation. Even if a short-term loads causes local damage to the wood matrix, this might not affect the stability in the long term since living trees are capable of self-healing and the production of reaction wood by stress-induced growth. The latter is related to phase field models for topology optimization based on stresses, see e.g. [8], [14].

2 A phase field model for the accumulation of residual stresses in trees

In the present work, the topology of the green wood is described by the phase field parameter φ. For voids it adapts the values $\varphi \approx -1$ and $\varphi \approx 1$ in regions of material. The transition zone (diffuse interface) the model defines the cambium layer of the tree by a lower threshold value $\overline{\varphi}_\mathrm{l}$ and an upper threshold value $\overline{\varphi}_\mathrm{u}$ of the phase field variable. The zone is essential in this model, since the cambial layer generates the secondary growth in the thickness direction of trees. The maturation of cells in the cambial layer leads to the accumulation of residual stresses. The topology in the model is based on an objective function F_1 in the direction $\boldsymbol{d}_\theta$ of primary growth (see Fig. 1)

$$F_1 = \int_{\mathcal{B}} -|\boldsymbol{d}_\theta|\,\varphi \;\mathrm{d}V = \int_{\mathcal{B}} \gamma_1(\boldsymbol{d}_\theta)\,\varphi \;\mathrm{d}V \quad \to \min \text{ w.r.t. } \varphi, \tag{1}$$

representing the tips of the plant. A second objective function F_2 accounts for stress-induced growth.

* Corresponding author: jan.wulf@tu-dortmund.de, phone +49 231 755-8954

Additionally, the inhomogeneity of stresses is measured by a stress component

$$\sigma_{\theta\theta} = \boldsymbol{d}_\theta \cdot (\boldsymbol{\sigma} \cdot \boldsymbol{d}_\theta), \tag{2}$$

in the direction of growth $\boldsymbol{d}_\theta$. These stresses define a difference to the arithmetic mean value

$$\overline{\sigma_{\theta\theta}} = \int_{\mathcal{B}} \frac{\sigma_{\theta\theta}}{V} \, \mathrm{d}V. \tag{3}$$

Finally, we set

$$\begin{aligned} F_2 &= \int_{\mathcal{B}} \frac{\overline{\sigma_{\theta\theta}} - \sigma_{\theta\theta}(\boldsymbol{\varepsilon}(\boldsymbol{u}), \varphi)}{\overline{\sigma_{\theta\theta}}} \, \varphi \, \mathrm{d}V \\ &= \int_{\mathcal{B}} \gamma_2(\overline{\sigma_{\theta\theta}}, \boldsymbol{u}, \varphi) \, \varphi \, \mathrm{d}V \quad \rightarrow \min \text{ w.r.t. } \boldsymbol{u}, \varphi, \end{aligned} \tag{4}$$

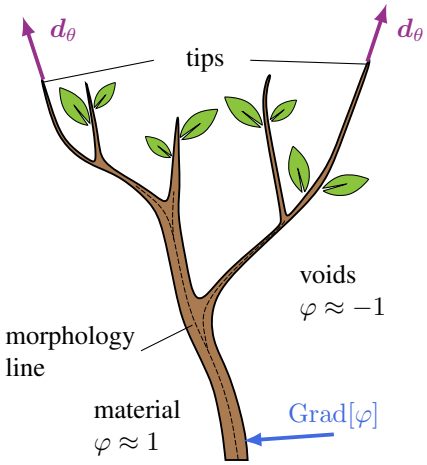

Fig. 1: Visual explanation of the primary growth direction $\boldsymbol{d}_\theta$. The gradient of the phase field variable Grad[φ] is corresponding to the stems surface.

as second objective function to account for stress-induced growth. In [1] such a stress-induced formation of material is called "reaction wood", which is distinguished between tension wood in angiosperms (hardwoods) and compression wood in gymnosperms (softwoods).

2.1 Morphological definition of the tip direction within the model

The tree morphology is influenced by its tropisms (phototropism, heliotropism, gravitropism, chemotropism e.g.), i.e. the ability of trees to adjust the growth direction of tips and roots as well as the curvatures of their branches in response to environmental stimuli such as changes in light intensity, movement of the sun, gravity or nutrient supply [11]. These are influences, which interact [4] and might also change over time shaping the topology of a tree almost inimitably. Therefore, the model works with the actual state of a tree structure mapping all tropisms with a predefined geometry. Based on Bresenham's line algorithm [2] growth directions are set for the rectangular elements in the regular finite element mesh common for phase field models. The slope of a function g defines the unit growth direction vector $\boldsymbol{d}_\theta$

$$\boldsymbol{d}_\theta = \begin{pmatrix} \dfrac{1}{\sqrt{(g')^2 + 1}} \\ \dfrac{g'}{\sqrt{(g')^2 + 1}} \end{pmatrix} \quad \text{with} \quad |\boldsymbol{d}_\theta| = 1. \tag{5}$$

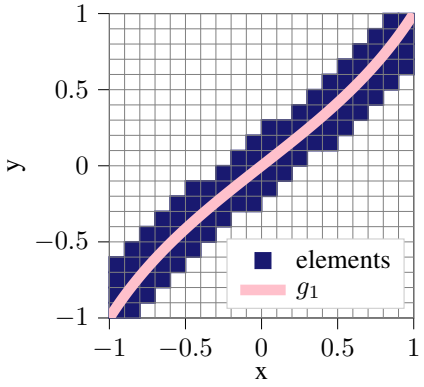

Fig. 2 Function $g_1(x)$ capturing elements in the regular rectangular finite element mesh with the line algorithm. For these elements a predefined growth direction is set. The thickness of the tip is set with a parameter in the algorithm.

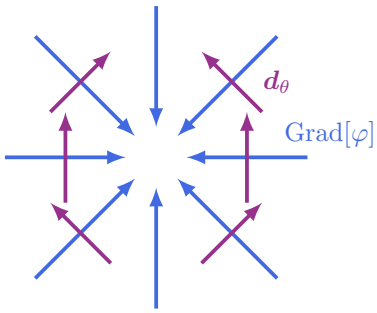

Fig. 3: Sample growth direction vectors $\boldsymbol{d}_\theta$ for new green wood nodes ($\varphi > \overline{\varphi}_\mathrm{u}$) based on the gradient of the phase field variable Grad[φ], which is always directed at right angles to the surface of the topology.

Example 2.1 A function 1 is given by $g_1(x) = \tan(1.7x)$ with $x \in \mathbb{R}$ and its derivative by $g_1{}'(x) = 1.7 \sec^2(1.7x)$, then the line algorithm captures elements of the regular rectangular finite element mesh as shown in Fig.2.

Furthermore, for all other nodes without an initial growth direction ($|\boldsymbol{d}_\theta| = 0$) that become wood material ($\varphi > \overline{\varphi}_\mathrm{u}$) through the evolution process in the transition zone, the phase field gradient is used to assign a fiber direction as shown in Fig.3. Since Grad[φ] is always directed perpendicular to the stems surface, it is rotated by $\beta = \pm\pi$ to ensure an upward growth direction

$$|\boldsymbol{d}_\theta| = 0, \ \varphi_n < \overline{\varphi}_\mathrm{u}, \ \varphi_{n+1} > \overline{\varphi}_\mathrm{u} : \quad \boldsymbol{d}_\theta = \begin{pmatrix} 0 & -\sin(\beta) \\ \sin(\beta) & 0 \end{pmatrix} \frac{\mathrm{Grad}[\varphi]}{|\mathrm{Grad}[\varphi]|}. \tag{6}$$

The growth direction vectors are set via additionally generated elements. In the finite element program, the values are then transferred to the Gauss points of the elements that actually belong to the system. To pass the Gauss point values for the fiber angle vector to the nodes, the error square method is used [16].

2.2 The phase field model

The phase field variable $\varphi \in \mathbb{R}$ describes the density distribution within the domain $\mathcal{B}$, defining the continuous function

$$f(\varphi) = \frac{e^{b(\varphi-1)}}{e^{b(\varphi-1)}+1} \qquad \rho = f(\varphi)\,\rho_0, \tag{7}$$

controlling the stiffness of green wood. This connects the displacement field and phase field variable in such a way that densities $0 \leq \frac{\rho}{\rho_0} \leq 1$ are created. Parameter b determines the slope of the function in the transition zone. We consider the strain energy density for linear elasticity

$$\Psi_{\mathrm{mech}}(\varepsilon,\varphi) = \frac{1}{2}\boldsymbol{\varepsilon}(\boldsymbol{u}) f(\varphi)\mathbf{C}\boldsymbol{\varepsilon}(\boldsymbol{u}). \tag{8}$$

At $\varphi = 1$ the function $f(\varphi)$ sets a limit for the stiffness of the material $\mathbf{C}$ and at $\varphi = 1$ a stiffness of almost 0 is conserved, which avoids singularities in the equation system. We use the double well potential

$$\Psi_{\mathrm{well}} = \varphi^6 - \varphi^4 - \varphi^2 + 1, \tag{9}$$

with minima at the preferred values of $\varphi = -1$ and $\varphi = 1$ to achieve a sharper resolution of material and voids. Furthermore we use the gradient energy density

$$\Psi_{\mathrm{Grad}} = \frac{1}{2}\mathbf{p}_d ||\mathrm{Grad}\varphi||^2, \tag{10}$$

governing the size of the transition zone, where the interface matrix

$$\mathbf{p}_d = L_c\,\mathbf{1} + p_s\,\mathrm{diag}(\boldsymbol{d}_\theta) \tag{11}$$

shapes the diffuse interface into the direction of growth. Parameter L_c, denoted as the interface parameter, accounts for a constant part, whereas p_s penalizes the vector $\boldsymbol{d}_\theta$ responsible for the growth direction based approach. The here introduced energy densities add up to the Ginzburg-Landau free energy density

$$\Psi_{\mathrm{int}}(\boldsymbol{\varepsilon},\varphi,\mathrm{Grad}[\varphi]) = \Psi_{\mathrm{mech}}(\boldsymbol{\varepsilon},\varphi) + \Psi_{\mathrm{well}}(\varphi) + \Psi_{\mathrm{grad}}(\mathrm{Grad}[\varphi]). \tag{12}$$

To give the model the urge to add densities in regions of predefined growth directions and in domains to compensate the normal stresses we incorporate the objective functions γ_1 and γ_2 into the total energy

$$\Pi = \int_{\mathcal{B}} \Psi_{\mathrm{int}}(\boldsymbol{\varepsilon},\varphi,\mathrm{Grad}[\varphi])\,\mathrm{d}V + \int_{\mathcal{B}} \gamma\varphi\,\mathrm{d}V - \int_{\mathcal{B}} f(\varphi)\rho_0\,\boldsymbol{b}\cdot\boldsymbol{u}\,\mathrm{d}V - \int_{\partial\mathcal{B}} (\bar{\boldsymbol{t}}\cdot\boldsymbol{u} + y\,\varphi)\,\mathrm{d}A, \tag{13}$$

united in one variable $\gamma = c_{\gamma,1}\gamma_1 + c_{\gamma,2}\gamma_2$ and penalized with the so called "nucleation densities" $c_{\gamma,1}$ and $c_{\gamma,2}$. The term $\gamma\,\varphi$ is identified as the external driving force shaping the topology. Then the Euler-Lagrange equations result in the balance of linear momentum and the balance of the phase field

$$\mathrm{Div}[\boldsymbol{\sigma}] + f(\varphi)\rho_0\,\boldsymbol{b} = 0, \tag{14}$$

$$\eta - \mathrm{Div}[\mathrm{Grad}[\varphi]\cdot\mathbf{p}_d] - f(\varphi)\rho_0\,\boldsymbol{b}\cdot\boldsymbol{u} + \gamma = 0 \qquad \eta := \frac{\partial\Psi_{\mathrm{int}}}{\partial\varphi}, \tag{15}$$

with the partial derivative of the inner energy with respect to the phase field variable η. In order to ensure the initial equilibrium state and to force an immediate change in the phase field the balance equation is extended by the rate of phase field variable φ

$$\eta - \mathrm{Div}[\mathrm{Grad}[\varphi]\cdot\mathbf{p}_d] - f(\varphi)\rho_0\,\boldsymbol{b}\cdot\boldsymbol{u} + \gamma = -\omega\dot{\varphi}, \tag{16}$$

penalized with the kinetic coefficient ω accounting for the speed of the evolution process. Applying the Galerkin method on Eq.(14) and Eq.(15) yields

$$\begin{aligned}\delta\Pi = \int_{\mathcal{B}} \Big[f(\varphi)\boldsymbol{\varepsilon}(\boldsymbol{u})\mathbf{C}\boldsymbol{\varepsilon}(\boldsymbol{\delta u}) + \eta\delta\varphi + \mathrm{Grad}[\varphi]\cdot\mathbf{p}_d\cdot\mathrm{Grad}[\delta\varphi]\Big]\,\mathrm{d}V + \int_{\mathcal{B}} (\gamma + \omega\dot{\varphi} - f'(\varphi)\rho_0\,\boldsymbol{b}\cdot\boldsymbol{u})\delta\varphi\,\mathrm{d}V \\ - \int_{\mathcal{B}} f(\varphi)\rho_0\,\boldsymbol{b}\cdot\delta\boldsymbol{u}\,\mathrm{d}V - \int_{\partial\mathcal{B}^{\boldsymbol{u}}_N} \bar{\boldsymbol{t}}\cdot\boldsymbol{\delta u}\,\mathrm{d}A - \int_{\partial\mathcal{B}^{\varphi}_N} y\,\delta\varphi\,\mathrm{d}A \overset{!}{=} \mathbf{0} \qquad \boldsymbol{u} = \overline{\boldsymbol{u}}\ \text{on}\ \partial\mathcal{B}^{\boldsymbol{u}}_D \quad \varphi = \overline{\varphi}\ \text{on}\ \partial\mathcal{B}^{\varphi}_D.\end{aligned} \tag{17}$$

Due to the non-linearity of phase field parameter φ, the equation is solved with a Newton Algorithm containing an implicit Euler time integration scheme. The rate of φ is defined by the summation of time increments Δt within a Newton step following

$$\varphi_{t_{n+1}} = \varphi_{\Delta t_{n+1}} + \varphi_{t_n} = \dot{\varphi}_{t_{n+1}} \Delta t + \varphi_{t_n} \quad \Rightarrow \dot{\varphi}_{t_{n+1}} = \frac{1}{\Delta t}(\varphi_{t_{n+1}} - \varphi_{t_n}). \tag{18}$$

2.3 Accumulation of residual stresses

The maturation of the cambium cells (tissue layer between bark and sapwood) into xylem cells (wood cells) leads to a hardening of the material in a rather short time and to a natural tendency to shrink in the longitudinal direction and to expand in the transverse direction [13]. Due to the bond between the new maturing cambium layer and the already stiff sapwood cells, the maturation elongation is limited. This leads to tensile growth stresses in longitudinal direction.

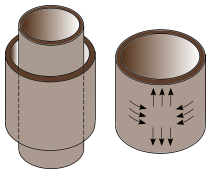

Fig. 4 Illustration of a maturing cambium cell. Maturation forces the cell to expand in transverse direction and to shrink in longitudinal direction, which is called "maturation strain". Due to the adhesion of the new layer to the already matured sapwood, longitudinal tension and transverse compression is accumulated, which is called "maturation stress". In radial direction however, the strain is nearly completely released.

The maturation strains are genetically predisposed and vary from species to species. In the model it is an input parameter. It is therefore important to determine the genetically predisposed maturation strain for the tree in advance. As Gril, J., Jullien, D., Bardet, S. *et al.* [6] show, this can be achieved with a strain gauge. By carving the trees surface strains are released and measured. This should only be done representatively, as it is an intervention in the tree's protective mechanism against moisture penetration and thus rot and fungi [15].

The local strain state in the cambial layer is manifested as a local reference state

$$\overline{\varphi}_{\mathrm{u}} > \varphi > \overline{\varphi}_{\mathrm{l}} \qquad \boldsymbol{\varepsilon}_h^{(t)} = \overline{\boldsymbol{\varepsilon}}_0 + \Delta \boldsymbol{\varepsilon}^{(t)}, \tag{19}$$

with the genetically predisposed maturation strain $\overline{\boldsymbol{\varepsilon}}_0$ in the cambial layer and the change in the integral strain state $\Delta \boldsymbol{\varepsilon}^{(t)}$ at time t. The strain state of all xylem layers ($\varphi > \overline{\varphi}_{\mathrm{u}}$) are defined by the strain history and the change in the integral strain state within this layer

$$\varphi > \overline{\varphi}_{\mathrm{u}} \qquad \boldsymbol{\varepsilon}_h^{(t)} = \boldsymbol{\varepsilon}_h^{(t-1)} + \Delta \boldsymbol{\varepsilon}^{(t)}. \tag{20}$$

2.4 Transverse isotropic wood material

Due to the anisotropic cell walls wood material in general has a microstructure with a preferred orientation. For this reason, we use transverse isotropy for the material in the model. Two isotropic transverse directions identify five independent material parameters.

$$E_1, \quad E_2 = E_3, \quad \nu_{12} = \nu_{13} = \nu, \quad G_{12} = G_{13}, \quad G_{23}. \tag{21}$$

These parameters are inserted into the stress-strain relation for linear elasticity reduced to the plane strain situation

$$\begin{bmatrix} \sigma_{11} \\ \sigma_{22} \\ \sigma_{12} \end{bmatrix} = \begin{bmatrix} C_{11} & 2\nu_{12}(\zeta + G_{23}) & 0 \\ & \zeta + 2G_{23} & 0 \\ & & G_{12} \end{bmatrix} \begin{bmatrix} \varepsilon_{11} \\ \varepsilon_{22} \\ 2\varepsilon_{12} \end{bmatrix}, \tag{22}$$

with parameters

$$C_{11} = \frac{1 - \nu_{23}}{1 - \nu_{23} - 2\nu_{12}\nu_{21}} E_1 \qquad \zeta = \frac{\nu_{12}\nu_{21} + \nu_{23}}{(1 - \nu_{23} - 2\nu_{12}\nu_{21})(1 + \nu_{23})} E_2. \tag{23}$$

The introduction of a fiber angle for the 2D case $\tan\theta = \frac{\boldsymbol{d}_\theta(2)}{\boldsymbol{d}_\theta(1)}$ corresponding to the growth direction is essential for the transversely isotropic material model, as the fiber angles are contained in a transformation tensor $\mathbf{T}(\theta)$ aligning the material matrix in Voigt's notation $\boldsymbol{C}^V$ with the preferred direction

$$\overline{\boldsymbol{C}}^V = \mathbf{T}(\theta)^T \boldsymbol{C}^V \mathbf{T}(\theta). \tag{24}$$

3 Growth of a branch with a delayed loading

parameter	.sym	value	unit
density	ρ	833	$\frac{\text{kg}}{\text{m}^3}$
Young's modulus L	E_1	1.00×10^4	MPa
Poisson's ratio	ν	0.30	[–]
interface exponent	b	5	[-]
nucleation density 1	c_{γ_1}	200	MPa
nucleation density 2	c_{γ_2}	0	MPa
interface parameter 1	L_c	3.00×10^{-2}	[-]
interface parameter 2	p_s	0.10	[-]
Young's modulus R	E_2	1000	MPa
shear modulus LR	G_{12}	1000	MPa
shear modulus RC	G_{23}	300	MPa
gen. pred. strain	$\overline{\varepsilon_0}$	5.00×10^{-3}	[-]

Table 1: Material parameters of *Fagus sylvatica* (common beach) in green condition [9], [7], [5], [10]

Our numerical example considers a neutral topology initialized with voids $\varphi_0 = -1$ except a small domain representing the beech sprout, where the phase field variable is set to $\varphi_0 = 1$ for a part of the growth distance, shown in Fig.5. For the material a common beach wood is used with the parameters of Tab.1. Due to the anisotropic fibers the Young's modulus in L-direction is 10 times higher than in the transverse R-direction. The finite element mesh uses 20253 rectangular elements with quadratic Ansatz functions.

Fig.6 shows the topology evolution over time in months. The objective functions result in the shape of a branch fork. At time step $t = 500$, the stress distribution of the component $\sigma_{\theta\theta}$ in $\boldsymbol{d}_\theta$ direction in section $\boldsymbol{\xi}$ (cf. Fig.5b) is given by Fig.7a.

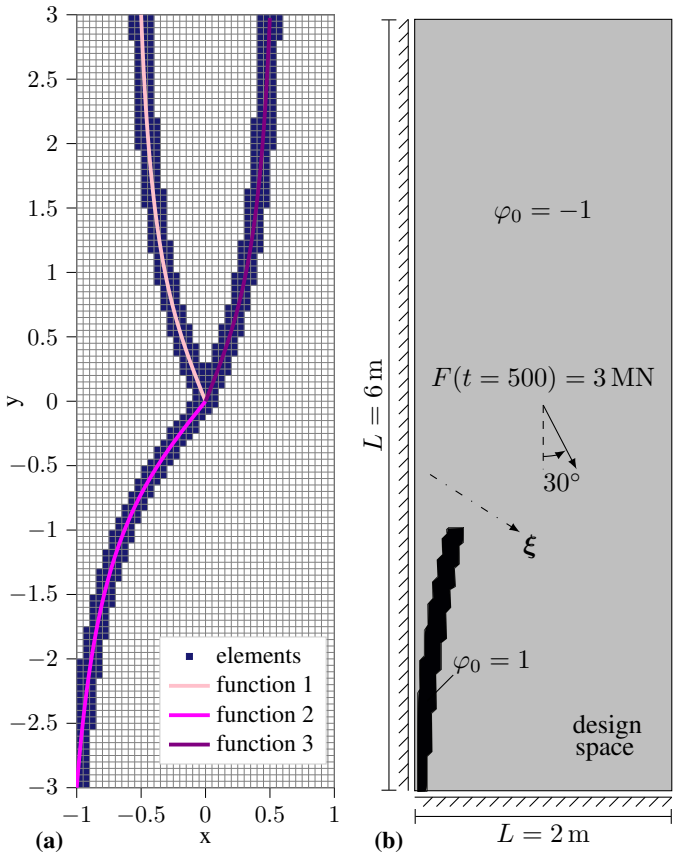

Fig. 5: **(a)** Discretization of the domain with morphological definition input via three functions. **(b)** Design space with symmetric boundary condition at $x = -1$.

A residual stress curve develops with tensile stress at the stems surface and compressive stress near the pith as shown in Fig.7a. Due to the soft transitions from material to void there is also a drop in the magnitude of the stresses towards the surface. After $t = 500$ an external force shown in Fig.5b is added to the system and the evolution continues. Immediately after the load is applied, the stresses in the defined section changes as shown in Fig.7a. A tension and a compression side is obtained. At time $t = 800$ the stem cross-section shows the stress distribution Fig.7b. We observe that newly maturing layers still put the stems surface under tensile stresses, which helps to stabilize the fibrous structure of the stem and protects the stems surface from compressive stresses. After $t = 800$ the external force is lifted, which results in the stress distribution shown in Fig.7c. A new cambial layer manifests itself in a stress state influenced by the external force. Thus, the unloading no longer has a significant influence on the stress curve.

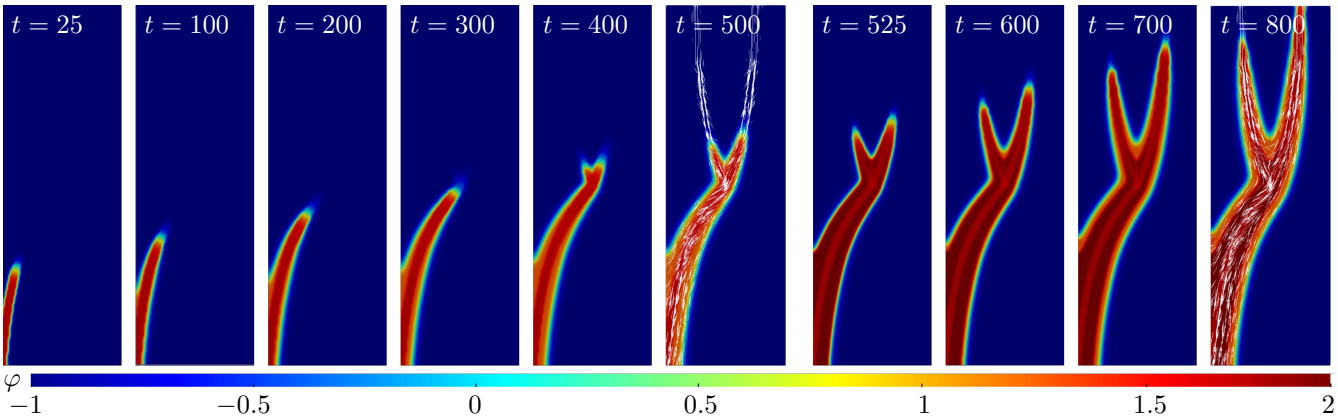

Fig. 6: Evolution of the phase field variable φ. The most convenient unit for pseudo time t is months. The objective functions shape the topology. At time t=500 an external force is added to the structure. Thin white lines indicate the direction of the growth vectors $\boldsymbol{d}_\theta$.

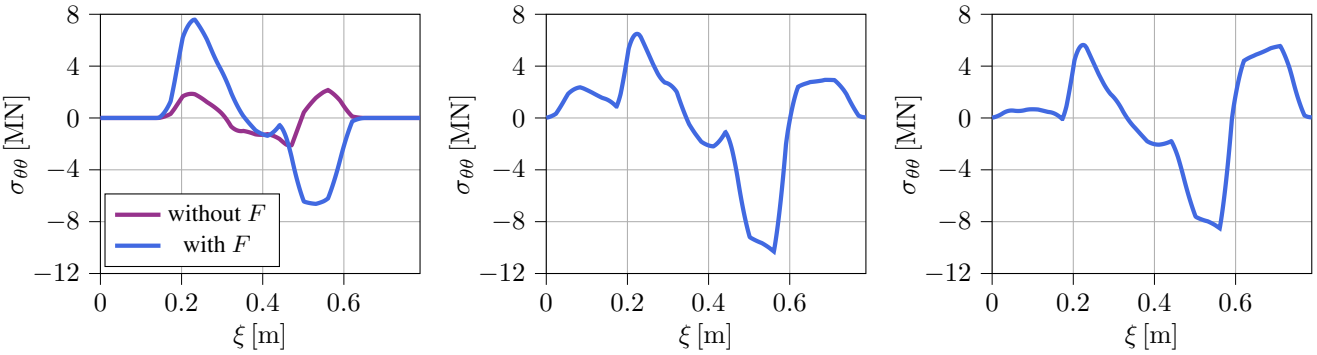

(a) $t = 500$ **(b)** With loading, $t = 800$ **(c)** After unloading, $t = 800$

Fig. 7: Stress component $\sigma_{\theta\theta}$ at different time steps

4 Conclusion

The introduction of a genetically predisposed maturation strain and the use of a strain history field leads to an accumulation of residual stresses as desired. Using the method presented in Section 2.3, the maturation strain can be adapted to individual trees. The interface matrix controls the ratio of primary and secondary growth and can also be individually adjusted to individual tree geometries. Defining a growth direction by the specification of a morphology line enables the model to simulate total stress situations of arbitrary topologies including branch forks. In combination with an experimental and probabilistic approach, this prepares the basis for an improved safety concept in tree engineering. As an outlook, the model will benefit from using a viscoelastic material behaviour with the mapping of the relaxation process, providing improved stress curves.

Acknowledgements Open access funding enabled and organized by Projekt DEAL.

References

[1] Bamber, R.K.: A general theory for the origin of growth stresses in reaction wood: how trees stay upright. Iawa Journal **22**(3), 205–212 (2001)
[2] Bresenham, J.E.: Algorithm for computer control of a digital plotter. IBM Systems journal **4**(1), 25–30 (1965)
[3] (Destatis), S.B.: Erläuterungen zum Indikator „Anstieg der Siedlungs- und Verkehrsfläche“. Publications of the Federal Statistical Office of Germany (2020). URL https://www.destatis.de/DE/Themen/Branchen-Unternehmen/Landwirtschaft-Forstwirtschaft-Fischerei/Flaechennutzung/Methoden/anstieg-suv.pdf. Accessed: 2022-09-30
[4] Firn, R., Myers, A.: Plant movements caused by differential growth—unity or diversity of mechanisms. In: P.W. Barlow (ed.) Differential Growth in Plants, pp. 47–55. Pergamon, Amsterdam (1989)
[5] Green, D.W., Winandy, J.E., Kretschmann, D.E.: Mechanical properties of wood. Wood handbook: wood as an engineering material. Madison, WI: USDA Forest Service, Forest Products Laboratory, 1999. General technical report FPL; GTR-113: Pages 4.1-4.45 **113** (1999)
[6] Gril, J., Jullien, D., Bardet, S., Yamamoto, H.: Tree growth stress and related problems. Journal of Wood Science **63**(5), 411–432 (2017)
[7] Lavers, G.: The Strength Properties of Timbers. Bulletin (Forest Products Research Laboratory (Princes Risborough, England)). H.M. Stationery Office (1969)
[8] Muench, I., Gierden, C., Wagner, W.: A phase field model for stress-based evolution of load-bearing structures. International Journal for Numerical Methods in Engineering **115**(13), 1580–1600 (2018)
[9] Niklas, K.J., Spatz, H.C.: Plant Physics. University of Chicago Press, Chicago (2012)
[10] Ross, R.J., et al.: Wood handbook: wood as an engineering material. USDA Forest Service, Forest Products Laboratory, General Technical Report FPL-GTR-190, 2010: 509 p. 1 v. **190** (2010)
[11] Roux, W.: Terminologie der Entwicklungsmechanik der Tiere und Pflanzen, vol. 9. Springer (1913)
[12] Steichele-Biskup, A.: Baumhaushotels in Deutschland (2022). URL https://www.adac.de/reise-freizeit/reiseplanung/inspirationen/deutschland/baumhaushotels/. Accessed: 2022-09-30
[13] Thibaut, B., Gril, J., Fournier, M.: Mechanics of wood and trees: some new highlights for an old story. Comptes Rendus de l’Académie des Sciences - Series IIB - Mechanics **329**(9), 701–716 (2001)
[14] Wulf, J.B., Muench, I.: Topology evolution of composite structures based on a phase field model. PAMM **20**(1), e202000163 (2021)
[15] Zeller, M., Münch, I.: Befestigung von Bauwerken in Bäumen mit Baumankern und doppelter Umreifung. Bautechnik **99**(S1), 13–22 (2022)
[16] Zienkiewicz, O., Taylor, R., Taylor, R.: The Finite Element Method: The basis. Butterworth-Heinemann (2000)